

APPROXIMATE PERFORMANCE ANALYSIS OF WIRELESS ULTRAVIOLET LINKS

Zhengyuan Xu

Dept. of Electrical Engineering
University of California
Riverside, CA 92521
dxu@ee.ucr.edu

ABSTRACT

The wireless ultraviolet (UV) communication technology has received great attention for either short-range high data-rate services or medium-to-large range low-rate sensing applications. However, performance of a UV link is limited by multiple constraints from the current UV laser source and detector technology, and atmospheric link conditions. This paper analyzes performance of both line of sight (LOS) and non-line of sight (NLOS) UV links in terms of signal to noise ratio and bit error rate of the detector. Roles of different parameters, such as data rate, communication range, transmitter power, beam and focal angle, receiving angle and field of view, are studied. Receiving powers for two typical links demonstrate square and linear decaying laws with respect to the communication range respectively. Compared with an LOS link, an NLOS link significantly degrades detection performance from one up to three orders of magnitude for the range from hundreds of meters down to meters.

INDEX TERMS

Ultraviolet, line of sight, non-line of sight, link budget, solar blind.

1. INTRODUCTION

Unlike a wireless radio frequency (RF) or microwave link, a wireless optical link offers potential advantages [8], such as huge unlicensed bandwidth, low-power and miniaturized transceiver, higher power densities, high resistance to jamming, and potential increase of data rate. Additionally, directional laser transmission and receiver's variable field-of-view (FOV) permit multiple accesses by different optical transceivers with minimal interference. Compared with the widely applied infrared technology in the wireless optical domain, the ultraviolet (UV) frequency band is much larger. Thus a UV link can potentially provide high data rate services. It also provides superior non-line of sight (NLOS) operability because of unique medium scattering and absorption by abundant atmospheric channel constituents, often of dimension comparable to the UV wavelength [12].

Ultraviolet is not a single entity, but consists of a very wide band of wavelengths. It is usually defined as electromagnetic wavelengths between 4nm and 400nm [12], which are the closest to the shortest wavelength of visible light, and much shorter than infrared. Ultraviolet spectrum can be loosely divided into near ultraviolet (NUV): 400~300nm, middle ultraviolet (MUV): 300~200nm,

far ultraviolet (FUV): 200~100nm and extreme ultraviolet (EUV): 100~4nm. The NUV includes wavelengths found in solar ultraviolet, and EUV is strongly absorbed by air.

Throughout the wide UV spectrum, the MUV range is a primary focus for wireless UV communications [17]. First, the solar radiation observed outside the atmosphere shows a wavelength-dependent energy distribution due to the constituents of the Sun [12]. Only about 9% is responsible for the whole UV region where only about less than 1% is in the MUV. Second, to reach the Earth's surface, the solar radiation must traverse Earth's atmosphere and loses energy by absorption and scattering. The relatively high transmission occurs for the longer wavelengths, and much stronger absorption is observed for the UV. The attenuation becomes appreciable and increases rapidly toward shorter wavelengths. Although, due to scattering, sky radiation may produce a very significant amount of MUV (strictly speaking below 280nm) reaching the Earth, larger attenuation together with the strong absorption of ozone causes the MUV region to be solar blind. By operating in this region, a UV photodetector with a large field of view (FOV) can maximally collect optical power with negligible background radiation. Thus it can achieve excellent signal-to-noise ratio (SNR) [12] and approach quantum-limited photon-counting detection, significantly superior to an infrared receiver. Similar to infrared or RF/microwave, UV radiation safety enforces UV exposure power limits [5], [12]. For continuous UV exposure, it is $0.1\mu\text{W}$ per cm^2 , and for less than 7-hour exposure, it is $0.5\mu\text{W}$ per cm^2 . So UV related experimentation and communication system design should follow these safety regulations.

However, benefits of UV cannot be realized in practical UV systems without technological advances in both miniaturized low-power solid-state UV devices and advanced UV communication technology. The development of low-power, low-cost UV communication has been impeded for decades after the pioneering work [16], [23] due to the lack of compact, low-power light sources and detectors. But recent advances in the solid-state devices such as laser emitting diodes (LEDs) and photodetectors [1], [2], [3], [4], [14], [15] open a new horizon for UV system development. With a strong extinction coefficient and unique scattering and absorption propagation mechanism through an atmospheric channel [10], [11], [16], the UV spectrum is ideal for diverse short-range communication environments, including line-of-sight (LOS) and NLOS communication channels [17], [22]. Although extensive field measurements have been carried out and various results have been reported [7], [9], [16], [20], [21], [19], [23], comprehensive understanding of UV communication especially analytical study still stays in its infancy.

In this paper, we rely on some experimental findings and part of analytical results in [6], [16], [23] to derive LOS and NLOS UV link equations in order to analytically reveal detection performance in different communication environments. We expect

This work was supported in part by the Army Research Office under Contract W911NF-06-1-0364, the Department of Defense under the Defense University Research Instrumentation Program (DURIP) Contract W911NF-06-1-0173, and the U. S. Army Research Laboratory under the Collaborative Technology Alliance Program, Cooperative Agreement DAAD19-01-2-0011.

our results will help to realistically bound dimensions of UV applications. Through detailed derivations under some approximations, we find that received power of an LOS link follows a square range-decay law while that of an NLOS link abides by a linear range-decay law. For an NLOS link, the common volume of the transmitter (Tx) and receiver (Rx) is one of the primary factors that determines the strength of the received optical signal. It depends on the link geometry that is in turn a function of their focal angles, Tx beam angle and Rx FOV. Together with other parameters such as medium scattering and absorption coefficients, scattering phase function, detector collecting area, and quantum efficiency, its effects on direct detection and quantum-limit based receive signal to noise ratio (SNR) and bit error rate (BER) are thoroughly analyzed and numerically tested based on some reasonably practical parameter values. For a given BER, range-rate trade-offs are clearly demonstrated. An NLOS link exhibits a severe performance loss compared with an LOS link.

2. LINK PERFORMANCE

In order to perform qualitative and quantitative analyses, let us first derive link equations for LOS and NLOS wireless UV links involving different parameters to be defined. A diagram is presented in Figure 1. Denote by R the data rate, P_t the transmitted power of the LED source including the electrical-optical efficiency, λ as the wavelength, Ω_1 as the solid angle of the transmitter (Tx) radiation cone, V as the Tx and receiver (Rx) common volume, r as the Tx and Rx separation, r_1 and r_2 as the distances of the common volume to the Tx and Rx respectively, θ_1 and θ_2 as the Tx and Rx focal angles, ϕ_1 and ϕ_2 as the Tx beam angle and Rx FOV, K_e the extinction coefficient that is related to the scattering coefficient K_s and absorption coefficient K_a by $K_e = K_s + K_a$, θ_s as the angle between forward direction of incident waves and observation direction, A_r as the area of the receiving aperture, η_r as the detector quantum efficiency, p_s the scattering phase function, and G the photomultiplication gain of the detector (for example, avalanche photodiode - APD, or photomultiplier tube - PMT). Typically $G = 30\sim 50$ for APD, and $10^3\sim 10^5$ for PMT [8], while up to 10^6 gain for commercial PMTs has been reported respectively by Hamamatsu Photonics, K.K., and Perkin Elmer [4]. Since the propagation mechanism is different for LOS and NLOS UV links, we will discuss them separately. According to [8] and [16], the received powers for LOS and NLOS links will be derived next.

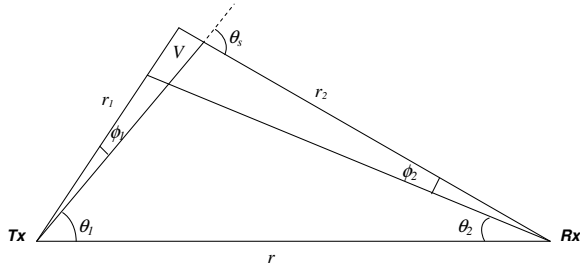


Fig. 1. An NLOS UV link.

2.1. LOS wireless UV link

According to [8], an LOS link undergoes an exponential attenuation by the atmosphere in addition to free space power decay. The free space path loss is inversely proportional to r^2 as $(\frac{\lambda}{4\pi r})^2$. The atmospheric attenuation can be expressed by $e^{-K_e r}$. The receiving gain of the detector is $\frac{4\pi A_r}{\lambda^2}$. Combining these factors, the

received optical power through an LOS link can be expressed as

$$P_{r,LOS} = P_t \left(\frac{\lambda}{4\pi r}\right)^2 e^{-K_e r} \frac{4\pi A_r}{\lambda^2}. \quad (1)$$

After simplification, it becomes

$$P_{r,LOS} = \frac{P_t A_r}{4\pi r^2} e^{-K_e r}. \quad (2)$$

Some observations can immediately be made. First, the power is only implicitly dependent of the wavelength through K_e . This parameter is sensitive to weather conditions as well [16]. Its effect may be pronounced for medium-to-large range (as r increases). Second, it decreases in proportion to r^2 , which is typically less severe than an RF link whose power decay exponent can be as large as 4. Assume the bandwidth of the detector is limited to twice of the data rate. Denote Planck constant by h , and speed of light by c . Then for direct detection, the quantum-limit based receive SNR becomes [8]

$$SNR_{r,LOS} = \frac{\eta_r G P_{r,LOS}}{2Rhc/\lambda}. \quad (3)$$

Notice that the definition of SNR follows typical ones (the ratio of signal power over noise variance [8]) instead of signal current over noise standard derivation [6]. After substituting (2), it becomes

$$SNR_{r,LOS} = \frac{\eta_r \lambda G P_t A_r}{8\pi r^2 h c R} e^{-K_e r}. \quad (4)$$

The BER for detection of on-off keying (OOK) signals is given by [6], [8]

$$BER_{r,LOS} = Q\left(\frac{\sqrt{SNR_{r,LOS}}}{2}\right) = \frac{1}{2} \operatorname{erfc}\left(\frac{\sqrt{SNR_{r,LOS}}}{2\sqrt{2}}\right), \quad (5)$$

where $Q(\cdot)$ and $\operatorname{erfc}(\cdot)$ are Q-function and complementary error function respectively.

According to (4) and (5), the range, rate and BER are related. So range-rate tradeoffs can be numerically studied.

2.2. NLOS wireless UV link

For an NLOS link, a step-by-step analysis as [16] will provide us a result for the final received optical power. For a given transmitted power P_t , the power per solid angle is P_t/Ω_1 . Then considering the path loss and attenuation, the received power density at distance r_1 becomes $\frac{P_t}{\Omega_1} \frac{e^{-K_e r_1}}{r_1^2}$. From this source at distance r_1 , the secondary sources due to scattering from atmospheric constituents (acting as a large number of tiny relay stations) in the common volume are established and amplified by $\frac{K_s}{4\pi} p_s V$. After this point, the propagation mechanism from the common volume to the receiver is similar to the LOS link. Those factors include the free space path loss $(\frac{\lambda}{4\pi r_2})^2$, atmospheric attenuation $e^{-K_e r_2}$, and the receiving gain of the detector $\frac{4\pi A_r}{\lambda^2}$. Combining all of the above, we obtain the following received power

$$P_{r,NLOS} = \left(\frac{P_t}{\Omega_1}\right) \left(\frac{e^{-K_e r_1}}{r_1^2}\right) \left(\frac{K_s}{4\pi} p_s V\right) \left(\frac{\lambda}{4\pi r_2}\right)^2 e^{-K_e r_2} \frac{4\pi A_r}{\lambda^2}. \quad (6)$$

Notice that p_s is a function of θ_s and takes different forms for isotropic, Rayleigh and Mie scattering models [16]. It is found that $\Omega_1 = 2\pi[1 - \cos(\phi_1/2)]$ [8], $\theta_s = \theta_1 + \theta_2$, $r_1 = r \sin \theta_2 / \sin \theta_s$,

$r_2 = r \sin \theta_1 / \sin \theta_s$. For small V , it takes a form $V = r_2 \phi_2 (r_1 \phi_1)^2$ [23]. After substituting V , θ_s , r_1 and r_2 , (6) becomes

$$P_{r,LOS} = \frac{P_t A_r K_s p_s \phi_2 \phi_1^2 \sin(\theta_1 + \theta_2)}{32\pi^3 r \sin \theta_1 (1 - \cos \frac{\phi_1}{2})} e^{-\frac{K_e r (\sin \theta_1 + \sin \theta_2)}{\sin(\theta_1 + \theta_2)}}. \quad (7)$$

It is interesting to note that the received power $P_{r,NLOS}$ is inversely proportional to r instead of r^2 as in $P_{r,LOS}$. This result for short range is also observed in [13],[17]. Without turbulence, the direct detection and quantum-limit based receive SNR and BER have the same forms as (3) and (5) after replacing $P_{r,LOS}$ by $P_{r,NLOS}$. With turbulence, the average BER instead of BER can be similarly defined after incorporating the distribution of irradiance (see p. 463 of [6]).

Although a number of factors have been considered in our analysis, there are still considerable practical constraints arising from devices and environments that limit the data rate. For this reason, the above results are very optimistic (and also approximate). For example, the beam divergence is much larger for an LED than for a UV lamp, significantly lowering the radiated power density. Conversely, their modulation bandwidths are at orders of GHz and 100kHz respectively. Besides the mean gain and active area, detectors bandwidth and dark current affect performance as well [2],[8]. Commercial APDs have bandwidth of GHz, gain of tens to hundreds, 10mm² area, and large dark current, while PMTs exhibit 100MHz bandwidth, 10⁶ average gain (high responsivity), 2cm² area, and extremely low dark current. The operational environment and conditions clearly pose additional constraints on the data rate. For a typical NLOS link, the common volume is approximated under a small value assumption. The precise analysis for an arbitrary geometry and size can be carried out by deploying a prolate spheroidal coordinate system, that was introduced by Reilly [16] and later on applied in [13],[18]. However, high complexity is anticipated. Meanwhile, model selection for the scattering phase function highly depends on additional assumptions. It should incorporate multipath scattering effects. These parts constitute future topics to further investigate. Even under an approximation, the derived link equations can still provide some useful insights into link performance, and guidelines to system design. Those findings will further help to realistically bound the dimensions of UV applications.

3. SIMULATION STUDY

To study link performance quantitatively, let's input typical figures of parameters in the analytical results. Assume isotropic scattering ($p_s = 1$) and no turbulence. Use 10 of 24-element LED arrays [20], each radiating 0.5mW optical power [1]. The LED electro-photo efficiency is only about 0.3%. OOK modulation is assumed. Other parameters are set as: $\lambda = 265nm$, $\eta_r = 0.2$, $G = 100$, $A_r = 1.8cm^2$ [2], $K_e = 0.79km^{-1}$, $K_s = 0.91^{-1}$, [16], $\theta_1 = 45^\circ$, $\theta_2 = 60^\circ$, $\phi_1 = 1^\circ$, $\phi_2 = 60^\circ$. Figure 2 demonstrates the rate-range-BER performance for both LOS and NLOS links. BER ranges from 10⁻¹ to 10⁻¹⁰ from the top to the bottom corresponding to each of ten curves in each subplot. For an LOS link with BER requirements of 10⁻³ (voice service) and 10⁻⁶ (data service), data rate can achieve 6Gbps and 2Gbps for 10m range, 50Mbps and 20Mbps for 100m range, and 300kbps and 100kbps for 1km range respectively. For an NLOS link with the same BER requirements, data rate can achieve 8Mbps and 3Mbps for 10m range, 700kbps and 300kbps for 100m range, and 20kbps and 9kbps for 1km range. There are at least three orders of magnitude rate decreases. According to additional simulation, if the gain G reduces to 1, data rate roughly reduces by a factor of 100

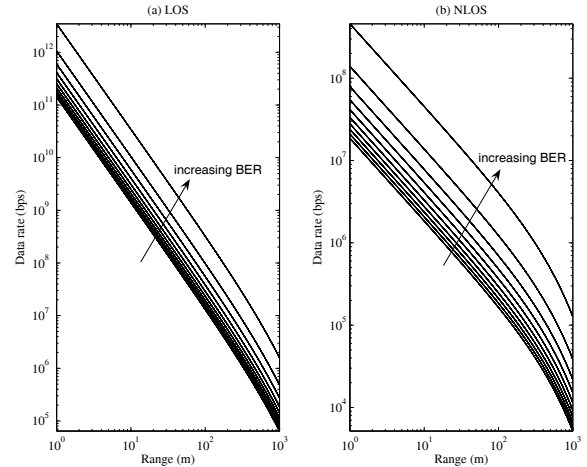


Fig. 2. Typical range-rate-BER performance of LOS and NLOS UV links.

for each case. As G increases, the data rate increases by an order of G . When turbulence is present, additional SNR is required to achieve the same BER performance as the free space case (see p. 464 of [6]). At the mean BER of 10⁻³, performance degrades by less than 1dB for weak to medium turbulence, about 3dB for strong turbulence, while at 10⁻⁶ BER, they increase to 3dB and 6dB respectively.

For an NLOS link, we continue to demonstrate effects of different parameters for a fixed BER of 10⁻³. Figure 3 shows effects of the Tx focal angle θ_1 increasing from 10^o to 80^o. For a large θ_1 , performance degrades due to longer propagation path thus more loss, while the common volume remains relatively unchanged. The effects of Rx focal angle θ_2 are demonstrated in Figure 4. Performance is not as sensitive as to θ_1 . This is because the large Rx FOV increases the common volume as θ_2 increases although path loss may increase due to longer path. The effects of Tx beam angle ϕ_1 are presented in Figure 5. It is observed that the performance is insensitive to ϕ_1 . It seems not surprising since an NLOS UV link relies on abundant medium scattering. As ϕ_1 increases, the common volume increases although the power density decreases. This can be observed from (7) that has a factor $\frac{\phi_1^2}{1 - \cos \frac{\phi_1}{2}} = \frac{\phi_1^2}{2 \sin^2 \frac{\phi_1}{4}}$. For $\phi_1 \in [0, \frac{\pi}{2}]rad$, this function changes slowly with Tx beam angle ϕ_1 . However, the performance is very sensitive to Rx FOV ϕ_2 , as shown by Figure 6. As ϕ_2 increases, more energy is collected, and detection performance improves.

4. REFERENCES

- [1] Solar-blind UV LED source, Sensor Electronic Technology, <http://www.s-et.com>
- [2] UV Photodiode and APDs, Hamamatsu Photonics, K.K., <http://www.hamamatsu.com>
- [3] UV light source and photodetector, Spectral Products LLC, <http://www.spectralproducts.com>
- [4] UV light source and detector, <http://www.roithner-laser.com/>, <http://www.nichia.com>, <http://www.perkinelmer.com>, <http://www.photonsystems.com>, <http://www.markettechinc.net>
- [5] Standard: IEC 60825-12:2005, Safety of laser products - Part 12: Safety of free space optical communication systems used for transmission of information.
- [6] L. Andrews and R. L. Phillips, *Laser Beam Propagation through Random Media*, 2nd ed., SPIE Press, 2005.

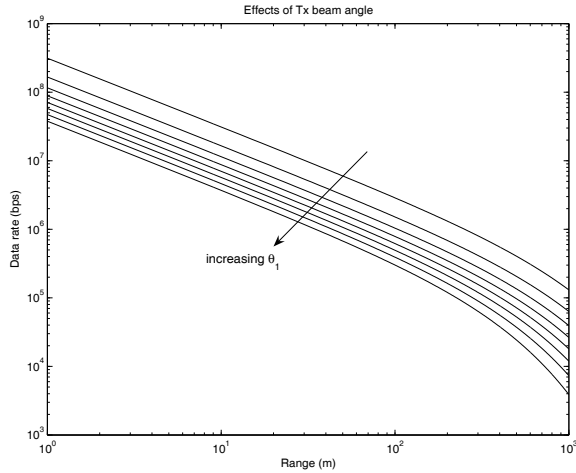


Fig. 3. Effects of Tx focal angle on performance of an NLOS link.

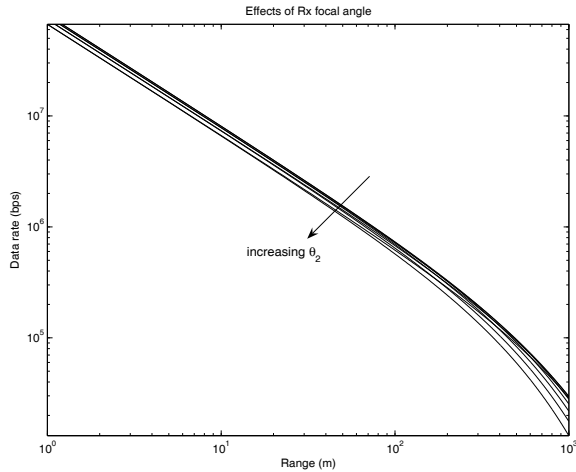


Fig. 4. Effects of Rx focal angle on performance of an NLOS link.

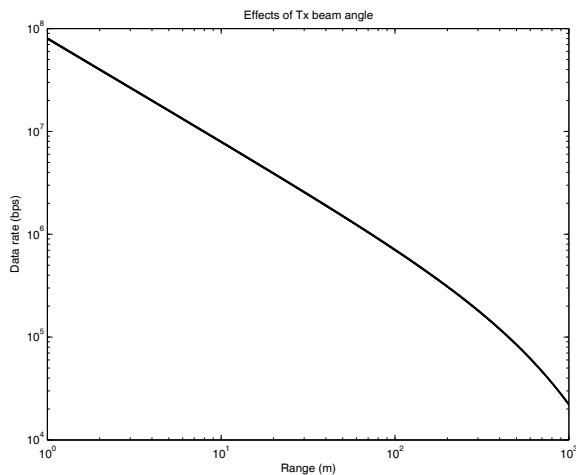


Fig. 5. Effects of Tx beam angle on performance of an NLOS link.

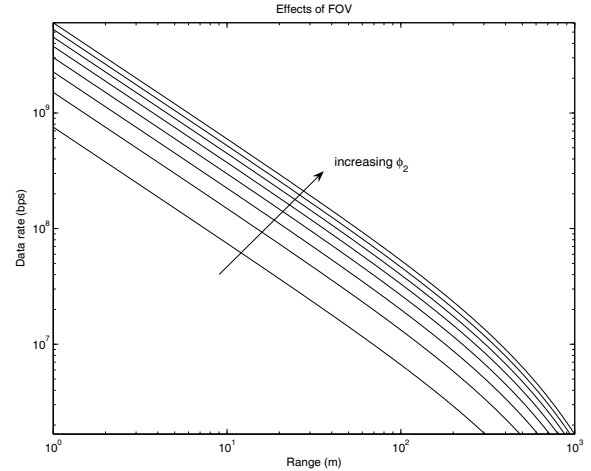


Fig. 6. Effects of Rx FOV on performance of an NLOS link.

- [7] S. Chang, J. Yang, J. Yang, Y. Lan, and H. Jia, "The experimental research of UV communication," *Proc. of SPIE*, vol. 5284, pp. 344-348, 2004.
- [8] R. M. Gagliardi and S. Karp, *Optical Communications*, 2nd ed., John Wiley & Sons, New York, 1995.
- [9] H. Jia, J. Yang, S. Chang, and H. Yin, "Study and design on high data rate UV communication system," *Proc. of SPIE*, vol. 6021, pp. 6021O.1-6021O.7, 2005.
- [10] S. Karp, R. M. Gagliardi, S. E. Moran, and L. B. Stotts, *Optical Channels: Fibers, Clouds, Water, and the Atmosphere*, Plenum Press, New York, 1988.
- [11] J. R. Kerr, P. J. Titterton, A. R. Kraemer, and C. R. Cooke, "Atmospheric optical communications systems," *Proc. of the IEEE*, vol. 58, no. 10, pp. 1691-1709, Oct. 1970.
- [12] L. R. Koller, *Ultraviolet Radiation*, 2nd ed., John Wiley & Sons, New York, 1965.
- [13] M. R. Leuttgen, J. H. Shapiro, and D. M. Reilly, "Non-line-of-sight single-scatter propagation model," *J. of the Optical Society of America*, vol. 8, no. 12, pp. 1964-1972, Dec. 1991.
- [14] S. Nakamura, "Topical Review: InGaN-based violet laser diodes," *Semicond. Sci. Technol.*, vol. 14, pp. R27R40, 1999.
- [15] S. Nakamura, "III-V nitride-based LEDs and lasers: Current status and future opportunities," *Electron Devices Meeting*, pp. 9-11, Dec. 10-13, 2000.
- [16] D. M. Reilly, "Atmospheric optical communications in the middle ultraviolet," *M.S. Thesis*, MIT, Cambridge, MA, 1976.
- [17] D. M. Reilly, D. T. Moriarty and J. A. Maynard, "Unique properties of solar blind ultraviolet communication systems for unattended ground sensor networks," *Proc. of SPIE*, London, UK, October 2004.
- [18] D. M. Reilly and C. Warde, "Temporal characteristics of single-scatter radiation," *J. of the Optical Society of America*, vol. 69, no. 3, pp. 464-470, March 1979.
- [19] G. A. Shaw, J. Fitzgerald, M. L. Nischan, and P. W. Boettcher, "Collaborative sensing test bed and experiments," *Proc. of SPIE*, vol. 5101, pp. 27-38, 2003.
- [20] G. A. Shaw, A. M. Siegel, and J. Model, "Extending the range and performance of non-line-of-sight ultraviolet communication links," *Proc. of SPIE*, vol. 6231, pp. 62310C.1-62310C.12, 2006.
- [21] G. A. Shaw, A. M. Siegel, J. Model, and D. Greisokh, "Recent progress in short-range ultraviolet communication," *Proc. of SPIE*, vol. 5796, pp. 214-225, 2005.
- [22] G. A. Shaw, A. M. Siegel, and M. L. Nischan, "Demonstration system and applications for compact wireless ultraviolet communications," *Proc. of SPIE*, vol. 5071, no. 1, pp. 241-252, Sept. 2003.
- [23] D. E. Sunstein, "A scatter communications link at ultraviolet frequencies," *B.S. Thesis*, MIT, Cambridge, MA, 1968.